Redox Interaction of Cytochrome c_3 with [NiFe] Hydrogenase from *Desulfovibrio vulgaris* Miyazaki F[†]

Naoki Yahata,[‡] Takashi Saitoh,[‡] Yuki Takayama,[‡] Kiyoshi Ozawa,[§,⊥] Hideaki Ogata,[∥] Yoshiki Higuchi,[∥] and Hideo Akutsu*[,‡]

Institute for Protein Research, Osaka University, Yamadaoka, Suita 565-0871, Japan, Faculty of Engineering, Yokohama National University, Hodogaya-ku, Yokohama 240-8501, Japan, and Graduate School of Life Science, University of Hyogo, Koto, Kamigori, Hyogo 678-1297, Japan

Received July 21, 2005; Revised Manuscript Received August 25, 2005

ABSTRACT: Cytochrome c_3 isolated from a sulfate-reducing bacterium, *Desulfovibrio vulgaris* Miyazaki F, is a tetraheme protein. Its physiological partner, [NiFe] hydrogenase, catalyzes the reversible oxidoreduction of molecular hydrogen. To elucidate the mechanism of electron transfer between cytochrome c_3 and [NiFe] hydrogenase, the transient complex formation by these proteins was investigated by means of NMR. All NH signals of uniformly ^{15}N-labeled ferric cytochrome c_3 except N-terminus, Pro, and Gly73 were assigned. ^{1}H-^{15}N HSQC spectra were recorded for ^{15}N-labeled ferric and ferrous cytochrome c_3, in the absence and presence of hydrogenase. Chemical shift perturbations were observed in the region around heme 4 in both oxidation states. Additionally, the region between hemes 1 and 3 in ferrous cytochrome c_3 was affected in the presence of hydrogenase, suggesting that the mode of interaction is different in each redox state. Heme 3 is probably the electron gate for ferrous cytochrome c_3. To investigate the transient complex of cytochrome c_3 and hydrogenase in detail, modeling of the complex was performed for the oxidized proteins using a docking program, ZDOCK 2.3, and NMR data. Furthermore, the roles of lysine residues of cytochrome c_3 in the interaction with hydrogenase were investigated by site-directed mutagenesis. When the lysine residues around heme 4 were replaced by an uncharged residue, methionine, one by one, the K_m of the electron-transfer kinetics increased. The results showed that the positive charges of Lys60, Lys72, Lys95, and Lys101 around heme 4 are important for formation of the transient complex with [NiFe] hydrogenase in the initial stage of the cytochrome c_3 reduction. This finding is consistent with the most possible structure of the transient complex obtained by modeling.

Cytochrome c_3 (cyt c_3) is a small soluble protein ($M_r \sim$ 14 000) including four *c*-type hemes. It shows very low oxido-reduction (redox) potentials (about −300 mV in average), which are considered to be essential for sulfate respiration. The three-dimensional (3D) structures (*1* and references therein) and macroscopic and microscopic redox potentials (*1*−*3* and references therein) of cyt c_3 from various bacteria have been determined. To elucidate its functional role, the redox interaction between cyt c_3 and either its physiological or nonphysiological partners, such as hydrogenase, ferredoxin (*4*−*6*), flavodoxin (*7*−*10*), rubredoxin (*11*), nine-heme cytochrome *c* (*12*), high molecular weight cytochrome *c* (hmc) (*13*), and type-II cyt c_3 (*14*), has been investigated. The most extensively studied physiological partner is hydrogenase, which plays a central role in hydrogen metabolism. Hydrogenase catalyzes the reversible oxidoreduction of molecular hydrogen and proton ions, and therefore, cyt c_3 acts as an electron acceptor or donor. This is one of the core reactions in the hydrogen cycling model for energy production in the genus *Desulfovibrio* (*15*).

Hydrogenases have been classified into three families according to the metal compositions of their active centers, namely, [Fe], [NiFe], and [NiFeSe] hydrogenases. [NiFe] hydrogenase has been the most extensively investigated among them. The three-dimensional crystal structures of [NiFe] hydrogenase isolated from *Desulfovibrio vulgaris* Miyazaki F (*Dv*MF) (*16*), *Desulfovibrio gigas* (*Dg*) (*17*), *Desulfovibrio fructosovorans* (*Df*) (*18*), and *Desulfovibrio desulfuricans* ATCC 27774 (*Dd*A) (*19*); [NiFeSe] hydrogenase from *Desulfomicrobium baculatum* (*Dmb*) (*20*); and [Fe] hydrogenase from *D. desulfuricans* (*Dd*) (*21*) and *Clostridium pasteurianum* (*22*) have been determined. The [NiFe] hydrogenase from *Dv*MF is a heterodimer protein. Its small subunit ($M_r \sim$ 29 000) contains three iron sulfur clusters, proximal [4Fe4S], medial [3Fe4S], and distal [4Fe4S] ones, which are distributed linearly from the active site to the molecular surface. On the other hand, the large subunit ($M_r \sim$ 63 000) contains the Ni−Fe active center and the Mg binding site (*16*).

[†] This research was partly supported by grants from the Ministry of Education, Science, Technology, Sport and Culture of Japan.

* To whom correspondence should be addressed: Institute for Protein Research, Osaka University, Yamadaoka, Suita 565-0871, Japan. E-mail: akutsu@protein.osaka-u.ac.jp. Phone: +81-6-6879-8597. Fax: +81-6-6879-8599.

[‡] Osaka University.

[§] Yokohama National University.

[∥] University of Hyogo.

[⊥] Current address: Research School of Chemistry, Australian National University, Canberra, ACT 0200, Australia.

10.1021/bi0514360 CCC: $33.50
Published on Web 01/20/2006

Table 1: Synthetic Oligonucleotides Used for Site-Directed Mutagenesis[a]

mutation	synthetic oligonucleotide
K10M	5′(214)-GCC GAC GGT CTG ATG GAC AAG ACC-3′(240)
K15M	5′(229)-ATG GAC AAG ACC ATG CAG CCC GTG GTC-3′(255)
K26M	5′(262)-CAC TCG ACC CAC ATG GCC GTG AAG TGT G-3′(289)
K57M	5′(355)-GAC AAC ATG GAC ATG AAG GAC AAG TCC-3′(381)
K58M	5′(358)-AAC ATG GAC AAG ATG GAC AAG TCC GCC-3′(384)
K60M	5′(364)-GAC AAG AAG GAC ATG TCC GCC AAG GGC-3′(390)
K72M	5′(400)-GCC ATG CAT GAC ATG GGC ACC AAG TTC-3′(426)
K94M	5′(466)-GAC GCC GCC AAG ATG AAG GAA CTG ACG-3′(492)
K95M	5′(469)-GCC GCC AAG AAA ATG GAA CTG ACG GGC-3′(495)
K101M	5′(487)-CTG ACG GGC TGC ATG GGC TCC AAG TGC-3′(513)

[a] The numbers in parentheses are the sequence numbers according to ref *29*.

The site of interaction between cyt c_3 and hydrogenase has been studied for a few systems. The [Fe] hydrogenase from *Dd* and cyt c_3 from *D. vulgaris* Hildenborough (*Dv*H) have been investigated by means of biochemical methods (*23*, *24*) and by structural modeling on the basis of NMR[1] data (*25*). For the [NiFeSe] hydrogenase and octaheme cyt c_3 ($M_r \sim 26\,000$) system from *Desulfomicrobium norvegicum* (*Dmn*), a mutation of Y73E in the cyt c_3 has been examined, which induced a decrease in the interaction (*26*, *27*). A structural modeling study has also been carried out on the interaction between [NiFe] hydrogenase and cyt c_3 from *DdA* (*19*), but no experimental evidence was provided.

We have determined the 3D solution structure of ferrous cyt c_3 from *Dv*MF using the NMR method (*2*), in which resonance assignments of the NH groups of cyt c_3 were established. The assignments for ferric cyt c_3 were performed in this work. Taking advantage of these assignments, chemical shift perturbations were measured to identify the interaction sites between cyt c_3 and hydrogenase in the oxidized and reduced states. Then, modeling of the cyt c_3−[NiFe] hydrogenase complex was carried out using a rigid-body docking algorithm, ZDOCK (*28* and references therein), and NMR data. Furthermore, the cyt c_3 overexpression in *Shewanella oneidensis* provided the effective production of site-directed mutant proteins. To determine the roles of surface residues of cyt c_3 in the transient complex formation, electron-transfer kinetics were analyzed for the wild-type and mutant proteins. The results provide a new insight into the mechanism of electron transfer between cyt c_3 and hydrogenase.

MATERIALS AND METHODS

Site-Directed Mutagenesis. All mutations were introduced into the pKFC3k plasmid, which contains the *Dv*MF cyt c_3 gene (*29*). Site-directed mutagenesis was conducted with a Mutan-Super Express Km kit (Takara Bio, Inc., Japan), and synthetic oligonucleotides were purchased from Invitrogen Co., Japan. The synthetic oligonucleotides used for the mutation at lysine residues are summarized in Table 1. The mutations were confirmed by nucleotide sequencing. This was performed with an ABI PRISM 310 genetic analyzer (Applied Biosystems Japan Ltd.) using a DNA sequence kit, BigDye Terminator Cycle Sequencing Ready Reaction (Applied Biosystems Japan Ltd.), and two M13 primers, RV-N and M4 (Takara Bio, Inc., Japan).

Purification of Cytochrome c_3. The wild-type and mutated cyt c_3 were overexpressed in *S. oneidensis* TSP-C as described previously (*30*). ^{15}N-Labeled cyt c_3 from *Dv*MF was overexpressed in *S. oneidensis* TSP-C using CHL medium (Chlorella Industry Co., Ltd., Japan) as described previously (*31*). Cyt c_3 was purified at 4 °C and pH 7.0. The sonicated cell suspension was centrifuged at 70 000*g* for 1 h. Ammonium sulfate was added to the supernatant to 50% saturation. After centrifugation at 70 000*g* for 30 min, ammonium sulfate was added to the supernatant to 70% saturation, followed by centrifugation for 40 min. The supernatant was applied to a HiLoad 26/10 phenyl sepharose HP column (Amersham Biosciences), which had been equilibrated with 30 mM sodium phosphate buffer 70% saturated with ammonium sulfate. Cyt c_3 fractions eluted with 70−0% saturation with $(NH_4)_2SO_4$ in 30 mM sodium phosphate buffer were collected and dialyzed against 30 mM phosphate buffer. Finally, the solution was applied to a HiLoad 26/10 SP Sepharose HP column (Amersham Biosciences), which was eluted with 0−300 mM NaCl. The cyt c_3 fractions were collected, dialyzed against ultrapure water, and then lyophilized. The purity was checked by SDS−polyacrylamide gel electrophoresis (SDS−PAGE).

To assign the ^{1}H-^{15}N resonances of ferric cyt c_3, amino acid-specific, ^{15}N-labeled cyt c_3 for Ala, Cys, Gly, His, Leu, Lys, Met, Phe, Ser, and Val was obtained from *Dv*MF, which was cultured using the chemical medium with amino acid mixture and purified as previously described (*4*, *32*).

Purification of [NiFe] Hydrogenase. *Dv*MF was cultured in medium C (*32*) in a 200-L anaerobic fermenter according to the reported method (*33*). The sonicated cell suspension was centrifuged at 143 000*g* for 1 h. The pellet was suspended in a 2-fold volume of 25 mM Tris-HCl buffer, pH 7.4, to which trypsin was added at the weight ratio of 0.0015 to the pellet. After the mixture was stirred for 12 h at 4 °C under nitrogen gas, trypsin inhibitor was added at the weight ratio of 0.625 to trypsin. The supernatant obtained by centrifugation at 143 000*g* for 1 h was subjected to dialysis. It was applied then to a DEAE TOYOPEARL 650S column (Tosoh, Japan), which was eluted with 25 mM Tris-HCl buffer, pH 7.4. The hydrogenase fractions were collected, concentrated, and applied to a HiLoad 26/60 Superdex 200 pg column (Amersham Biosciences), which was eluted with 50 mM NaCl and 25 mM Tris-HCl buffer, pH 7.4. Then, the purification on DEAE TOYOPEARL 650S and

[1] Abbreviations: NMR, nuclear magnetic resonance; HSQC, heteronuclear single-quantum coherence; TOCSY, total correlation spectroscopy; NOESY, nuclear Overhauser effect spectroscopy; HEPES, *N*-2-hydroxyethylpiperazine-*N*′-2-ethanesulfonic acid; rmsd, root-mean-square deviation.

HiLoad 26/60 Superdex 200 pg columns was repeated to obtain the purified [NiFe] hydrogenase.

NMR Sample Preparation. The sample solutions for the ^{1}H-^{15}N resonance assignments of ferric cyt c_3 included 1−2 mM cyt c_3 in 30 mM phosphate buffer, pH 7.0 or 6.0 (10% ^2H_2O). The sample solution for the chemical shift perturbation experiments comprised 0.4 mM cyt c_3 in 30 mM sodium phosphate buffer, pH 7.0 (10% ^2H_2O). To examine the effect of interaction, 0.6 and 0.4 mM hydrogenase were added to the oxidized and reduced cyt c_3, respectively. Fully reduced cyt c_3 was obtained by flushing hydrogen gas into the sample tube in the presence of a trace amount of hydrogenase (molar ratio, ca. 0.001). Chemical shifts are referred to an internal standard, 2,2-dimethyl-2-silapentane-5-sulfonate (DSS).

NMR Experiments. All NMR measurements were performed at 303 K with an AVANCE DRX-600 NMR spectrometer (Bruker, Germany). 3D TOCSY-HSQC and NOESY-HSQC experiments were performed for the sequence-specific assignment of the ferric cyt c_3 with 1024 (^{1}H) × 64 (^{15}N) × 128 (^{1}H) data points. The spectral widths were 16.93, 41.8, and 51.0 ppm in the ^{1}H, ^{15}N, and ^{1}H dimensions, respectively. The mixing times were 30, 75, and 100 ms for TOCSY-HSQC and 150 ms for NOESY-HSQC. ^{1}H-^{15}N HSQC spectra were recorded with 2048 (^{1}H) × 128 (^{15}N) data points. The spectral widths were 21 (^{1}H) × 40 (^{15}N) ppm for the oxidized sample and 18 (^{1}H) × 38 (^{15}N) ppm for the reduced one. Spectra were processed using a standard Bruker software, XWINNMR version 3.1, and analyzed using software packages NMR-Pipe and Pipp. The average chemical shift perturbation ($\Delta\delta_{ave}$) of each backbone amide was calculated using the equation, $\Delta\delta_{ave} = [\Delta\delta H^2 + (\Delta\delta N/5)^2]^{1/2}$, where $\Delta\delta$H and $\Delta\delta$N stand for the changes in the ^{1}H and ^{15}N chemical shifts, respectively. The values of $\Delta\delta_{ave} \geq 0.02$ and 0.05 ppm were categorized as large perturbations for the ferric and ferrous types, respectively. The minimum values (0.02 and 0.05 ppm) were determined by averaging all $\Delta\delta_{ave}$ values after removing $\Delta\delta_{ave}$ in the top 10% and bottom 10%.

Modeling of the Cytochrome c_3−[NiFe] Hydrogenase Complex. Modeling of the ferric cyt c_3−[NiFe] hydrogenase complex was performed using a rigid body protein−protein docking algorithm called ZDOCK. ZDOCK 2.3 optimizes the desolvation (DE), pairwise shape complementarity (PSC), and electrostatics (ELEC) by means of Fast Fourier Transform (FFT). All default parameters and a 6° rotational sampling interval were used. In this calculation, we used the coordinates of the crystal structures of ferric cyt c_3 (PDB code 1J0O) and hydrogenase (PDB code 1H2A). The water molecules in these PDB files were excluded, except for those bound to the Mg center. For cyt c_3, an amino acid residue whose solvent accessibility is high (>50% for either the main chain or side chain according to program NACCESS (*34*)) and NMR $\Delta\delta_{ave}$ is smaller than 0.01 ppm was defined as a noninteracting residue on the surface, which was blocked from the interaction in the docking calculation. Thus, NMR data were used to remove the unperturbed residues from the possible interaction sites on the surface of cyt c_3. For hydrogenase, metal centers were ignored in the calculation. From the top 100 solutions, biologically meaningful orientations in which the distance between heme 4 iron in cyt c_3 and the Fe1 atom of the distal [4Fe4S] cluster in the hydrogenase was smaller than 20 Å were selected. Then, similar orientations (backbone rmsd ≤ 2 Å) were grouped.

The protein complexes obtained were subjected to energy minimization using the X-PLOR 3.851 program (*35*). For normal residues and water molecules, force fields were applied to the complex structures based on the parameters of CHARMM 22. Heme group parameters were corrected at the positions of the thioether bonds with cysteine residues. For the metal centers in hydrogenase, the charges were assigned manually. Calculation according to the conjugate gradient method (*36*) was carried out for 1000 steps. Position restraints were applied to all atoms except those within 20 Å from heme 4 and the distal [4Fe4S] cluster. In addition to them, four hemes, iron sulfur clusters, and their ligands were also fixed.

Determination of Macroscopic Redox Potentials. The macroscopic redox potentials of mutated cyt c_3 were determined by differential pulse polarography (DPP). Polarograms were obtained with a 394 Digital Electrochemical Trace Analysis System (PerkinElmer, Inc.), which was controlled with Model 394 Analytical Voltammetry Software. The working electrode was a dropping mercury electrode, with a platinum wire coil as the counter electrode and an Ag/AgCl electrode as the reference electrode. The pulse height, scan rate, and drop time were 20 mV, 2 mV s^{-1}, and 2 s, respectively. Cyt c_3 was dissolved at about 0.1 mM in 30 mM sodium phosphate buffer (pH 7.0). The polarograms were fitted using an analytical equation for four consecutive one-electron reversible electrode reactions (*37*). Macroscopic redox potentials were referred to the standard hydrogen electrode (SHE) at 30 °C in this work.

Measurements of Cytochrome c_3 Reduction by Hydrogenase. Whenever a diluted hydrogenase solution for kinetic experiments was prepared, hydrogenase activity was determined as follows. A solution (1.5 mL) of 1 mM methyl viologen and 50 mM HEPES (pH 7.0) in an anaerobic cuvette was bubbled with high-grade hydrogen gas (purity rate, 99.99999% and over) for 30 min. The absorbance at 604 nm was measured as a function of time with a BECKMAN DU640 spectrophotometer after the addition of a small amount (final, 7 nM) of hydrogenase. The slope of the tangent at the beginning of the time course was used for calculation of the hydrogen oxidation rate. An absorption coefficient of 13 600 M^{-1} cm^{-1} for methyl viologen was used.

Anaerobic cuvettes were filled with a cyt c_3 solution at various concentrations (final, 1−30 μM) in 50 mM HEPES (pH 7.0). They were bubbled with high-grade hydrogen gas for 30 min. The change in absorbance at 552 nm ($\delta\epsilon_{552} = \epsilon_{552red} - \epsilon_{552ox} = 84\,000$ M^{-1} cm^{-1}) was measured after the addition of hydrogenase (final, 7 nM). The slope of the tangent at the beginning of the time course was used for calculation of the initial rate of reduction of cyt c_3, which was corrected using the [NiFe] hydrogenase activity determined previously. The K_m and k_{cat} of each cyt c_3 were determined by nonlinear least-squares fitting of the Michaelis−Menten equation to the experimental data.

RESULTS

^{1}H-^{15}N HSQC spectra of ferric and ferrous ^{15}N-labeled cyt c_3 are presented in Figure 1. ^{1}H-^{15}N resonance assignments

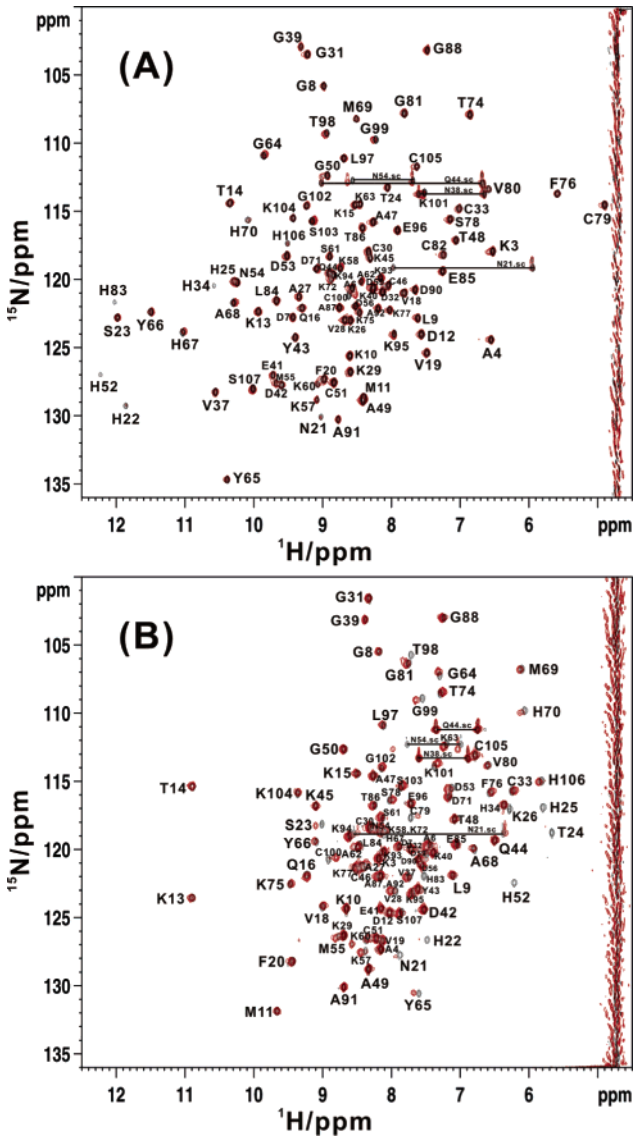

FIGURE 1: ^{1}H-^{15}N HSQC spectra of cytochrome c_3 in the absence (black) and presence (red) of [NiFe] hydrogenase at 600 MHz and 303 K. Assignments are given in the spectra. (A) Ferric and (B) ferrous cytochrome c_3.

for ferrous cyt c_3 have been reported (*2*). All ^{15}N and ^{1}H backbone signals except those of the N-terminus, Pro residues, and Gly73 in the fully oxidized state were assigned in this work by 3D NOESY-HSQC experiments. The NH signal of Gly73 was very broad, and this signal disappeared on measurement at 600 MHz. The NH signals of His35, Asn38, and Ala89 disappeared at pH 7.0. However, these signals were observed at pH 6.0 (His35, ^{1}H, 8.76 and ^{15}N, 121.0; Asn38, 9.96 and 126.4; Ala89, 8.65 and 126.7). Since His35 is coordinated to heme 2, its signal suffered from a significant paramagnetic effect. Asn38 and Ala89 are located on the surface. To identify the NH cross-peak of Ala, Cys, Gly, His, Leu, Lys, Met, Phe, Ser, and Val, amino acid-specific, ^{15}N-labeled proteins were used. In total, 98% of the proton resonances at backbone were assigned. The chemical shifts are deposited in the BioMagResBank with the accession number 6572.

To investigate the interaction of cyt c_3 with [NiFe] hydrogenase, the chemical shifts of ^{1}H-^{15}N HSQC cross-peaks of ferric ^{15}N-cyt c_3 were measured in the absence and

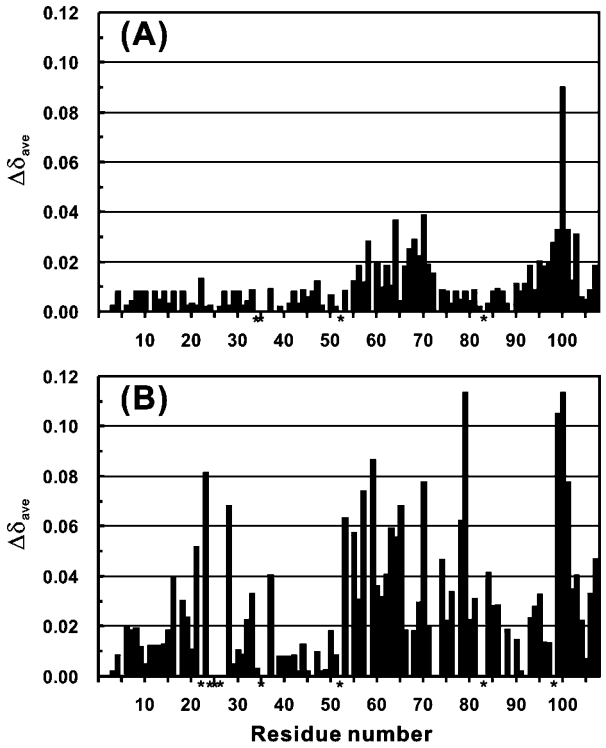

FIGURE 2: Average chemical shift perturbations of cytochromes c_3 observed in ^{1}H-^{15}N HSQC spectra in the presence of hydrogenase. (A) Ferric and (B) ferrous cytochrome c_3. Asterisks indicate residues not detected in the complex.

presence of oxidized [NiFe] hydrogenase, respectively (Figure 1A). The same measurement was carried out for ferrous ^{15}N-cyt c_3 and the reduced hydrogenase (Figure 1B). Chemical shift changes and broadening of resonances were observed in both cases. Average chemical shift perturbations ($\Delta\delta_{ave}$) were calculated from these spectra and are shown in Figure 2. Asterisks indicate the residues whose signals have either disappeared or shifted to a great extent. For the ferric type, Cys100 showed the largest shift. Cys100 is covalently linked to heme 4. Besides for Cys100, large shifts were also observed for Gly64, His70, Gly99, Lys101, and Ser103 ($\Delta\delta_{ave} > 0.03$ ppm). Compared to the $\Delta\delta_{ave}$ values for the ferric type, $\Delta\delta_{ave}$ values for the ferrous one were generally larger. In particular, Ser23, Asp59, Cys79, Gly99, and Cys100 showed large shifts ($\Delta\delta_{ave} > 0.08$ ppm). The resonances of His34, His35, His52, and His83 for the ferric type and His22, Thr24-Lys26, His35, His52, His83, and Thr98 for the ferrous type were lost in the presence of [NiFe] hydrogenase. These histidine residues are heme axial ligands. In the oxidized state, the line widths of these resonances were broader than those of the other resonances because of the paramagnetic effect. Furthermore, these heme axial ligands are not exposed on the surface of cyt c_3. The residues showing large chemical shift perturbations and that then disappeared were mapped in the crystal structure of ferric cyt c_3 (PDB code: 1J0O) and the 20-averaged solution structure of ferrous one (PDB code: 1IT1), respectively (Figure 3). For the ferric type, chemical shift changes were only observed around the heme 4 region. For the ferrous type, however, the residues between hemes 1 and 3 (Asn21−Lys26 and Val28) were affected in addition to the residues around heme 4 (Lys57, His70, Thr98, Gly99, Cys100, and Lys101).

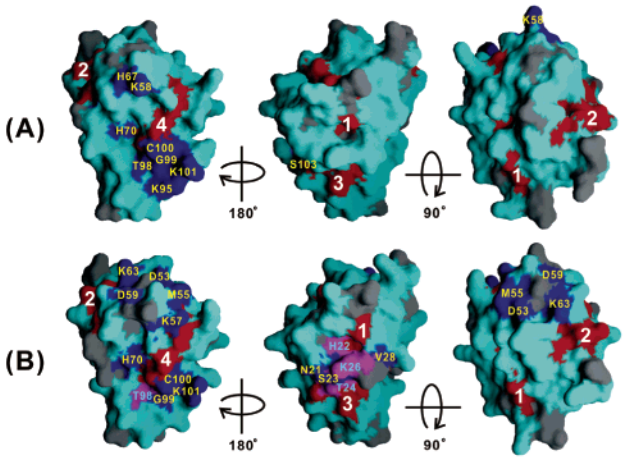

FIGURE 3: Chemical shift perturbation mapping of (A) ferric and (B) ferrous cytochrome c_3 on the crystal structure and the 20-averaged solution structure, respectively (PDB codes, 1J0O and 1IT1). Residues are colored according to the following classification: (A) $\Delta\delta_{ave} < 0.02$ ppm (cyan), $\Delta\delta_{ave} \geq 0.02$ ppm (blue); (B) $\Delta\delta_{ave} < 0.05$ ppm (cyan), $\Delta\delta_{ave} \geq 0.05$ ppm (blue). Unassigned residues, residues not detected in the complex, and hemes are colored gray, magenta, and red, respectively. Sequential numbers and heme numbers are given for the latter two. These figures were produced with GRASP (*44*).

To investigate the mode of interaction between cyt c_3 and [NiFe] hydrogenase in detail, modeling of the transient complex between cyt c_3 and [NiFe] hydrogenase in the oxidized state was performed using ZDOCK 2.3. At first, the noninteractive residues of cyt c_3 as to the interaction with hydrogenase were selected. The residues with $\Delta\delta_{ave} < 0.01$ ppm on the surface (high solvent accessibility) were regarded as the noninteractive ones. In total, 28 residues (K3, A4, A6, D7, G8, K10, D12, K13, K15, Q16, V19, S23, K26, A27, K29, D32, G39, E41, Q44, K45, G50, K75, K77, E85, T86, G88, A91, and K104) were selected and blocked from the interaction in docking calculation. Only the top 100 predictions were analyzed. The distribution of the predicted positions of cyt c_3 around hydrogenase is shown in Figure 4. Spheres represent the heme 4 iron positions of cyt c_3. On the basis of the structural architecture of metal centers, it has been suggested that the region near the distal [4Fe4S] cluster of hydrogenase interacts with the redox center of a counterpart and exchanges electrons (*17*). This was supported by mutational conversion of the [3Fe4S] cluster to the [4Fe4S] one (*38*). So the predicted complexes with heme 4 of cyt c_3 close to the distal [4Fe4S] cluster of hydrogenase (the distance between the heme 4 iron and the FE1 of the distal [4Fe4S] cluster, ≤20 Å) were selected. Thirty predicted complexes met this condition. Then, the selected complexes were grouped on the basis of docking orientations (backbone rmsd ≤ 2 Å). The orientation with the best ZDOCK rank in each group was regarded as a representative orientation. As a result, the 30 orientations were classified to seven groups. Then, energy minimization was performed for the seven representative complexes. The refined seven complex structures were numbered according to the energy rank. The characteristics of these seven final model structures are summarized in Table 2. The shortest iron−iron distance was found in structure no. 2 (13.6 Å). The distance between the edges of heme 4 and the distal [4Fe4S] cluster was compared for the structures nos. 1 and 2. The distances between the

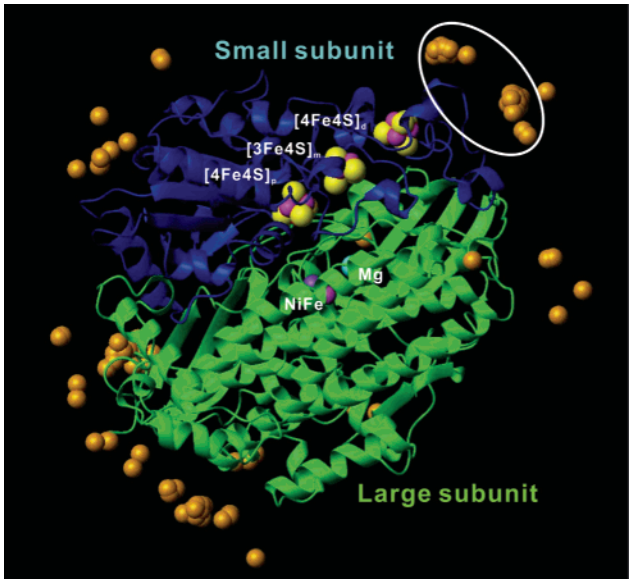

FIGURE 4: Spatial distribution of the top 100 docking positions. The heme 4 iron position of cytochrome c_3 is represented by an orange sphere. The polypeptide chains of the large and small subunits of hydrogenase are colored green and blue, respectively. Iron, sulfur, nickel, and magnesium in the metal centers are shown in magenta, yellow, purple, and cyan, respectively. The 30 predicted complexes whose distance between the heme 4 iron and the FE1 of the distal [4Fe4S] cluster is 20 Å or less are contained in the white circle.

Table 2: Properties of the Seven Final Model Structures for the Cytochrome c_3−[NiFe] Hydrogense Complex

no.	the best "zdock" rank in the group	Fe−Fe distance in heme/cluster (Å)[a]	interface accessible surface area of cyt c_3/hyd.[b] (Å^2)	percentage of polar/nonpolar atoms at interface[b] (%)	energy (electrostatic + vdW[c]) (kcal/mol)
1	26	14.4 (FE1)	907/882	40/60	−25086
2	8	13.6 (FE1)	717/681	47/53	−24948
3	68	17.6 (FE4)	861/757	38/62	−24909
4	67	14.3 (FE4)	571/594	39/61	−24883
5	78	15.3 (FE4)	984/961	43/57	−24621
6	19	16.3 (FE4)	820/827	35/65	−24592
7	4	16.6 (FE4)	967/929	45/55	−24381

[a] The numbers in parentheses indicate the atoms which are the closest to the heme 4 iron in the distal [4Fe4S] cluster. [b] These parameters were calculated at the website http://www.biochem.ucl.ac.uk/bsm/PP/server/. [c] vdW, van der Waals.

HMB3 atom of heme and the S1 atom of the cluster are 6.5 and 6.4 Å for nos. 1 and 2, respectively. Since they are similar to each other, these models can possibly be selected as the most possible structures of the cyt c_3−hydrogenase complex. These structures are shown in Figure 5. It should be indicated that in model no. 2, heme 4 is close to His188 of hydrogenase, which is one of the ligands of the [4Fe4S] cluster.

To determine the role of surface residues of cyt c_3 in the interaction with [NiFe] hydrogenase, 10 lysine residues, mainly around heme 4 (K10, K15, K26, K57, K58, K60, K72, K94, K95, and K101), were substituted by methionine, respectively. Two tyrosines, Y65 and Y66, around heme 4 were also mutated to Y65A and Y66L. The K26M mutant was prepared based on the results of the chemical shift perturbation experiment in the reduced state. There was no change in the UV−visible spectra of any mutant cyt c_3 in

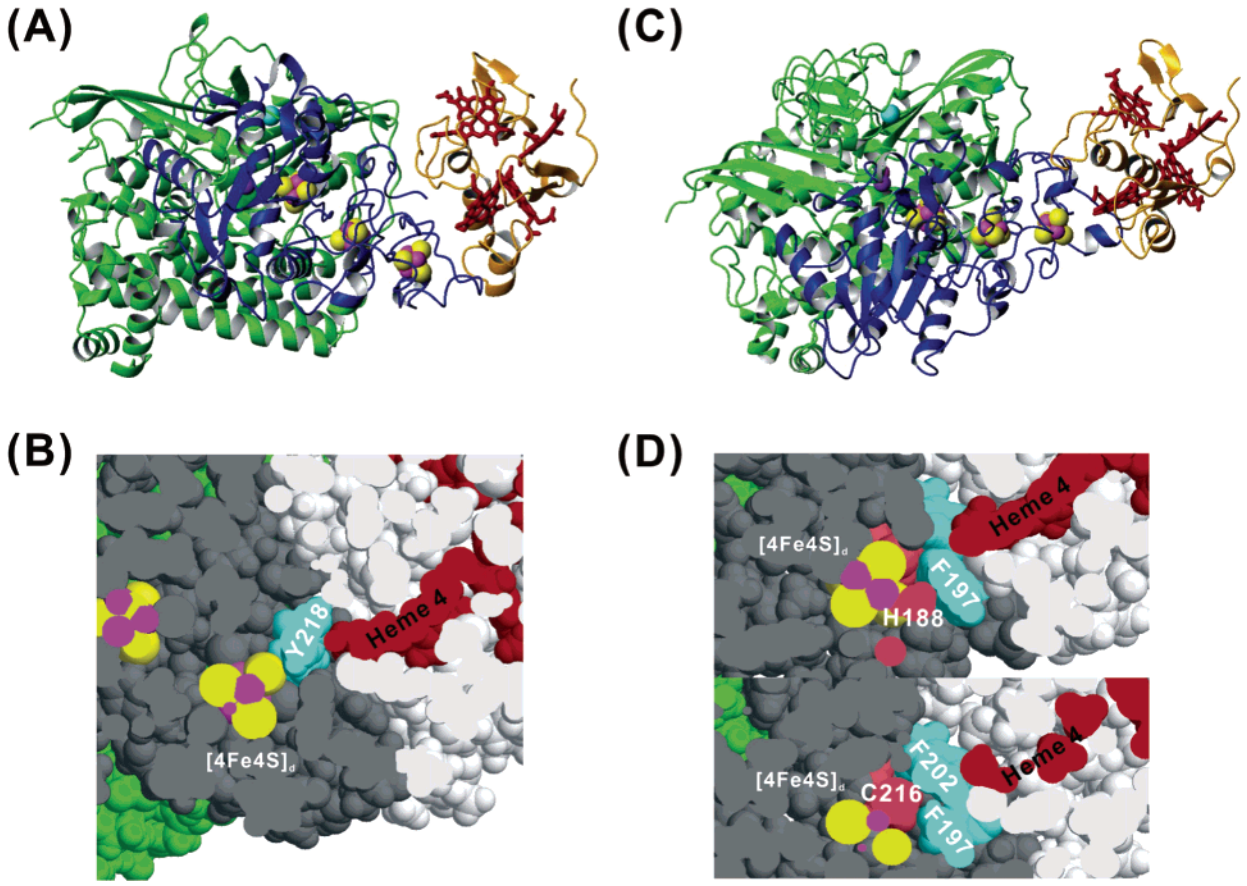

FIGURE 5: The most possible model structures of the ferric cytochrome c_3−[NiFe] hydrogenase complexes. (A and C) Overall structures of nos. 1 and 2 models, respectively. The polypeptide chains of cytochrome c_3 and the large and small subunits of hydrogenase are colored orange, green, and blue, respectively. Hemes are drawn as red sticks. Iron, sulfur, nickel, and magnesium in the metal centers are shown in magenta, yellow, purple, and cyan, respectively. (B and D) Interface region of nos.1 and 2 models, respectively. Cytochrome c_3 and the large and small subunits of hydrogenase are colored white, green, and gray, respectively. Hemes, irons, and sulfurs in the cluster are colored red, magenta, and yellow, respectively. Aromatic residues and ligands of the distal [4Fe4S] cluster which may be involved in the electron-transfer pathway are colored cyan and pink, respectively.

the fully oxidized and reduced states compared with those of the wild-type. In contrast, there were changes in their 1D ^{1}H NMR spectra for the oxidized forms. The heme methyl signals in the low field (13−32 ppm), which are labeled alphabetically (A−J) from low to high field, were assigned. The observed spectra are given in the Supporting Information. The signal of 18^1-CH_3 for heme 4 in K57M cyt c_3 showed the largest change (1.18 ppm) among the 10 lysine mutants. The four macroscopic redox potentials were determined by differential pulse polarography and are summarized in Table 3. The effects of the lysine mutations on the redox potentials were small (less than 10 mV).

The kinetics of reduction of cyt c_3 by hydrogenase in the presence of hydrogen gas were investigated for these proteins. The concentration of cyt c_3 was varied from 1 to 30 μM to determine the steady-state reduction rate by means of the Michaelis−Menten equation (Figure 6). The obtained kinetic parameters are summarized in Table 4. While k_{cat} was similar for all proteins, K_m changed with the mutation. The increase of K_m means the decrease of the affinity between cyt c_3 and hydrogenase. Given the k_{cat}/K_m values, the mutant cyt c_3 could be classified to three groups, namely, group i (unaffected, K10M, K26M, and Y65A), group ii (42−58%, K15M, K57M, K58M, Y66L, and K94M), and group iii (20−37%, K60M, K72M, K95M, and K101M). The largest decrease in activity was observed for K60M cyt c_3. Since k_{cat} is more or less constant, the k_{cat}/K_m ratio reflects the difference in K_m.

Table 3: The Macroscopic Redox Potentials of the Wild-Type and Mutated Cytochromes c_3 in 30 mM Sodium Phosphate Buffer (pH 7.0) at 30 °C (standard errors ± 2 mV)[a]

	$E_I^{o'}$	$E_{II}^{o'}$	$E_{III}^{o'}$	$E_{IV}^{o'}$
wild-type[b]	−242	−296	−313	−358
K10M	−235 (+7)	−289 (+7)	−306 (+7)	−349 (+9)
K15M	−250 (−8)	−294 (+2)	−315 (−2)	−352 (+6)
K26M	−240 (+2)	−296 (0)	−312 (+1)	−359 (−1)
K57M	−244 (−2)	−291 (+5)	−311 (+2)	−353 (+5)
K58M	−242 (0)	−294 (+2)	−313 (0)	−354 (+4)
K60M	−240 (+2)	−289 (+7)	−310 (+3)	−351 (+7)
Y65A[b]	−227 (+15)	−267 (+29)	−296 (+17)	−335 (+23)
Y66L[b]	−217 (+25)	−288 (+8)	−313 (0)	−358 (0)
K72M	−243 (−1)	−291 (+5)	−309 (+4)	−353 (+5)
K94M	−245 (−3)	−295 (+1)	−315 (−2)	−356 (+2)
K95M	−240 (+2)	−291 (+5)	−311 (+2)	−351 (+7)
K101M	−242 (0)	−293 (+3)	−311 (+2)	−353 (+5)

[a] $E_i^{o'}$ (i = I−IV) is the macroscopic redox potential at the ith reduction step relative to the standard hydrogen electrode (SHE). The values in the parentheses are the differences between wild-type and mutants. [b] From ref *31*.

DISCUSSION

This is the first case in which modeling of the cyt c_3−hydrogenase complex was carried out on the experimental

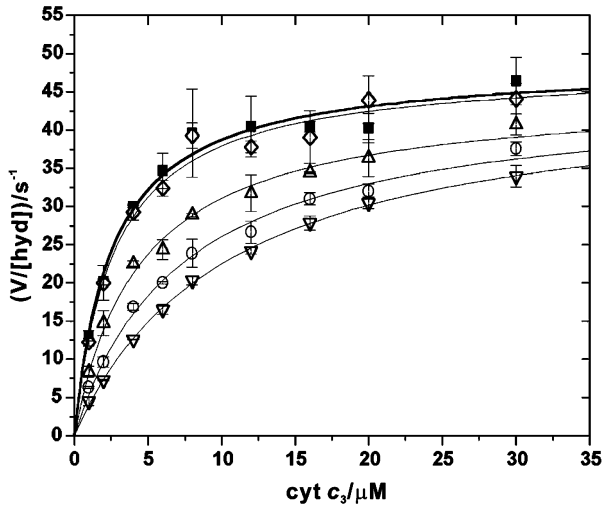

FIGURE 6: Rate of reduction of cytochrome c_3 as a function of its concentration in 50 mM HEPES buffer (pH 7.0) at 25 °C. The concentration of hydrogenase was 7 nM. Wild-type (■), K10M (◇), K15M (△), K60M (▽), and K95M (○). The thick line and thin lines are the curves fitted to the Michaelis−Menten equation for the wild-type and mutated cytochromes c_3, respectively.

Table 4: Kinetic Parameters of Electron Transfer between [NiFe] Hydrogense and Either the Wild-Type or Mutated Cytochromes c_3 in 50 mM HEPES Buffer (pH 7.0) at 25 °C

	K_m (μM)	k_{cat} (s^{-1})	k_{cat}/K_m (μM^{-1} s^{-1})[a]
wild-type	2.6 ± 0.3	49 ± 1	19
K10M	2.7 ± 0.3	48 ± 2	18 (i)
K15M	4.5 ± 0.4	45 ± 1	10 (ii)
K26M	3.0 ± 0.4	44 ± 1	14 (i)
K57M	5.1 ± 0.5	48 ± 2	9.4 (ii)
K58M	5.7 ± 0.5	45 ± 1	8.0 (ii)
K60M	10.4 ± 0.4	46 ± 1	4.4 (iii)
Y65A	2.2 ± 0.1	49 ± 1	23 (i)
Y66L	4.3 ± 0.5	47 ± 2	11 (ii)
K72M	6.7 ± 0.4	42 ± 1	6.4 (iii)
K94M	5.7 ± 0.3	45 ± 1	8.0 (ii)
K95M	7.3 ± 0.7	45 ± 2	6.2 (iii)
K101M	9.9 ± 0.9	51 ± 2	5.1 (iii)

[a] The parentheses show the grouping given in the text.

evidence for the proteins from the same bacterium. Chemical shift perturbation mapping suggested that the region around heme 4 is involved in the interaction with hydrogenase in the oxidized state (Figure 3). This is in good agreement with the previous reports on other systems (*4-8*, *11*−*14*). Since cyt c_3 possesses many lysine residues around heme 4 and hydrogenase is an acidic protein, this is reasonable from the electrostatic point of view. The pH-dependent, heme-specific redox potentials of *Dv*MF cyt c_3 were determined by means of electrochemical methods and NMR (*39*). At the first reduction step, the heme-specific redox potential of heme 4 is the highest at pH 7. So heme 4 is most suitable for accepting an electron from the electrochemical point of view. This supports the idea that heme 4 is the physiological interaction site in the electron transfer from hydrogenase to cyt c_3.

Modeling of the complex was carried out on the basis of chemical shift perturbations. In principle, we should have dealt with the ferric cyt c_3-reduced hydrogenase system to discuss the transient complex. However, it is extremely difficult in the NMR experiments. Since NMR data were determined under the ferric cyt c_3-oxidized hydrogenase

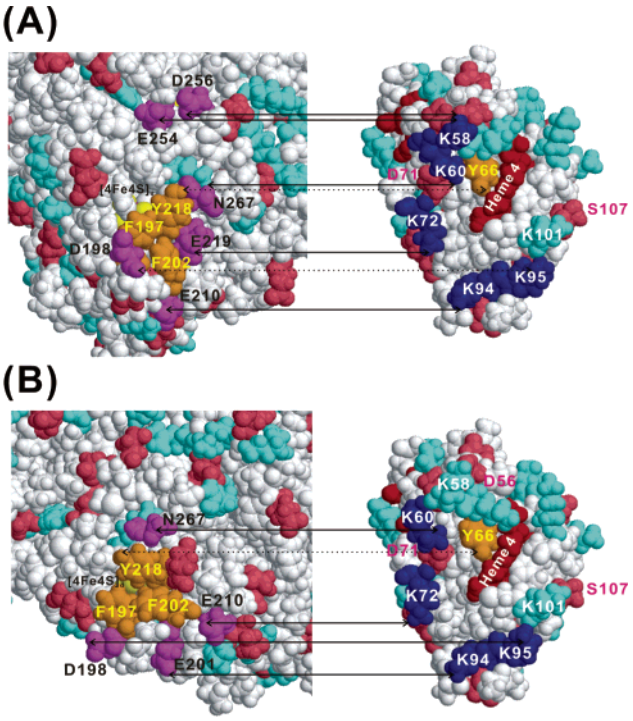

FIGURE 7: Open book views of nos. 1 (A) and 2 (B) cytochrome c_3−[NiFe] hydrogenase complex models, respectively. The cytochrome c_3 and [NiFe] hydrogenase faces are shown on the right and left, respectively. Hemes and sulfurs in the cluster are colored red and yellow, respectively. Positively charged residues (lysine and arginine) and negatively charged residues (glutamate and aspartate) are colored cyan and pink, respectively. Contact residues, which were affected by site-directed mutagenesis, are colored blue and magenta. Aromatic residues, which are suggested to be involved in the electron-transfer pathways, are colored orange. Bold and dotted arrows connect the paired residues which form either salt bridges or hydrogen bonds, respectively.

conditions, we used the oxidized hydrogenase structure in the docking analysis. This can be justified by the fact that at least the structure around the iron sulfur clusters in the reduced form is identical with that in the oxidized form (*40*).

As shown in Figure 7A, K58, K60, K72, and K94 in cyt c_3 form salt bridges with E254/D256, N267 (terminal carboxyl oxygen), E219, and E210 in the small subunit of hydrogenase, respectively, in model no. 1. Also, the K95 amino proton and Y66 OH form hydrogen bonds with the D198 carbonyl oxygen and Y218 OH, respectively. The latter would be important to fix the orientation of Y218 at the optimal position for electron transfer since the aromatic ring of Y218 would be involved in the electron-transfer pathway between the two proteins (Figure 5A). Furthermore, K60 and K101 form intramolecular salt bridges with D71 and S107 (terminal carboxyl oxygen) in cyt c_3, respectively (Figure 7A). For the model no. 2 (Figure 7B), on the other hand, K60, K72, K94, and K95 form salt bridges with N267 (terminal carboxyl oxygen), E210, E201, and D198 in the hydrogenase small subunit, respectively. Y66 OH forms a hydrogen bond with Y218 OH of the hydrogenase. Furthermore, K58, K60, and K101 form intramolecular salt bridges with D56, D71, and S107 (terminal carboxyl oxygen) in cyt c_3, respectively. The transient complex should be consistent with the effect of mutation on the hydrogen reduction kinetics. Namely, the residues in group iii (K60, K72, K95, and K101) in Table 4 should be involved in the interaction between the two proteins. In models nos. 1 and 2, the same

three residues of group iii (K60, K72, and K95) are involved in the interface interactions. This suggests both models satisfy the requirement to the same extent. K60M exhibited the largest increase in K_m (Table 4). Models nos. 1 and 2 show that this mutation not only removes a salt bridge but also leaves two negative charges in repulsion. This explains the largest increase in K_m. In group iii, K101 is the only residue which is not involved in the direct interaction in models nos. 1 and 2. K101 forms an intramolecular salt bridge with S107 in the complex, but it is free and exposed on the surface in the monomer. The positive charge of K101 would contribute to attract the hydrogenase to the interaction site. However, since it has no partner for a salt bridge in the hydrogenase, its long chain would become an obstacle for the close contact between the [4Fe4S] cluster and heme 4. The intramolecular salt bridge with the C-terminal carboxyl group would remove the long side chain from the interface. In the K101M mutant, the side chain of methionine cannot behave in this way, leading to the suppression of the complex formation. This would explain the decrease in the affinity between two proteins.

The iron−iron distance between two redox centers (14.4 and 13.6 Å for models nos. 1 and 2) is greater than those in the model structure for the cyt c_3−[Fe] hydrogenase (8.8 Å) and cyt c_{553}−[Fe] hydrogenase (12.3 Å) complexes (*25*, *41*). The distal [4Fe4S] cluster in the [NiFe] hydrogenase is more buried than that in [Fe] one. Although a pair of redox center edges at a distance of 14 Å can be used for a functional electron transfer (*42*), an aromatic residue would be helpful for effective electron transfer. In model no. 1, $[4Fe4S]_d$−Y218−heme 4 is the putative electron-transfer pathway. In model no. 2, two pathways ($[4Fe4S]_d$−H188−F197−heme 4 and $[4Fe4S]_d$−C216−F202−heme 4) are possible (Figure 5D). His188 and Cys216 are the ligands of the distal [4Fe4S] cluster. The His ligand is a unique structural characteristic for [NiFe] hydrogenase. His188 and Cys216 are conserved in a newly classified gene family of [NiFe] hydrogenase small subunit, *hynS* (*43*). Although the F202 and Y218 aromatic rings are not perfectly conserved in the [NiFe] hydrogenase gene, *hynS*, the F197 aromatic ring is perfectly conserved as either Phe or Tyr (*43*). Therefore, the pathway, distal [4Fe4S] cluster−His188−aromatic ring (F197), seems to be a conserved electron-transfer pathway for the reduction by [NiFe] hydrogenase. Actually, F192 (identical to F197 in *Dd*A sequence) was also assumed to be involved in the electron-transfer pathway in the model structure for the cyt c_3−[NiFe] hydrogenase complex from *Dd*A. The distances between heme 4 CMB and F192 CE1 and between F192 CE1 and distal [4Fe4S] cluster S3 were 4.5 and 4.4 Å, respectively (*20*). In our model no. 2, the distance between heme 4 CMB and F197 (which is sequentially identical to F192 in *Dd*A [NiFe] hydrogenase) CE1 and between F197 CE1 and H188 CE1 are 3.5 and 3.4 Å, respectively. So, our model no. 2 should be more effective for electron transfer. It was also suggested for *Dg* [NiFe] hydrogenase that the partially exposed His ligand of the distal [4Fe4S] cluster is the gate for electron transfer to cyt c_3 (*17*), since histidine is an unusual ligand for [4Fe4S] clusters. Our model no. 2 fits to this idea.

On the other hand, evaluation for the conservation of intermolecular salt bridges and hydrogen bonds is not straightforward because of the low homology in cyt c_3 amino acid sequence. *Dv*MF cyt c_3 is classified to the 2-4-2-4 group on the basis of heme attachment sites (*31*). In *hynS* genes from *Desulfovibrio* 2-4-2-4 species, E198, E201, E210, Y218, E219, and E254 are conserved. However, lysine residues of cyt c_3 belonging to the 2-4-2-4 group are not exactly conserved (*31*). Conserved residues in group ii and iii are Y66, K94, and K95. K58 and K72 are not conserved in the current sequence alignment. However, they are conserved in a way, because a lysine residue is located at the direct neighbor on the replacement by another residue. Although K60 is replaced by Gln in *Dd*E cyt c_3, it is compensated by the replacement of D71 by Thr, suggesting that they can form hydrogen bonds instead of salt bridges. Therefore, the amino acid residues involved in cyt c_3−hydrogenase interactions in models nos. 1 and 2 are reasonably conserved in the relevant sequences. In summary, both models nos. 1 and 2 are reasonably consistent with the mutation experiments and conformational requirements for electron transfer. However, model no. 2 is more favorable in terms of the short iron−iron distance, the genetically conserved electron-transfer pathway, and the involvement of His ligand in electron transfer.

One of the most important findings in this work is that the reduced cyt c_3 was more greatly and widely influenced by hydrogenase (Figure 3B) compared to the ferric type. This suggests that the affinity constant of the complex formation was larger for the reduced form than for the oxidized form. In the region around heme 4, Asp59, Gly99, and Cys100 showed the largest chemical shift changes, and the resonance of Thr98 disappeared (Figure 2B). This indicates that the residues close to heme 4 are also involved in the interaction with hydrogenase in the reduced state. However, the perturbed sites around heme 4 are more scattered in comparison with the oxidized one (Figure 3). An important point regarding the reduced state is the appearance of a new perturbed site around heme 3. The chemical shift perturbation at Cys79, which links heme 3, was one of the largest. The resonances of Asn21−Lys26 and Val28, which are situated between hemes 3 and 1, either disappeared or showed large perturbations (Figures 2B and 3B). These perturbations might indicate either a new interaction site with hydrogenase or secondary effects of binding on other sites. If the latter is the case, the binding site should be heme 4. Since the region around heme 3 was not affected in the oxidized state, this kind of secondary effect is unlikely. Therefore, the region around heme 3 would be the major interaction site for the electron transfer from cyt c_3 to hydrogenase. The microscopic redox potential of heme 3 is the lowest in the last reduction step at pH 7 (*39*). Therefore, heme 3 could be the gate for the electron supply to hydrogenase. Actually, the conformation of cyt c_3 including the region between hemes 1 and 3 changes on reduction (*2*). This conformational change would be an origin of the new interaction site. A large affinity constant will promote the electron transfer from cyt c_3 to hydrogenase even if the redox potential of the latter is lower than that of the former. The interaction site for the reduction of hydrogenase by cyt c_3, however, is a subject open for future investigations.

In conclusion, positive residues around heme 4 in cyt c_3 (K60, K72, K94, and K95) act in concert to interact with [NiFe] hydrogenase, in which aromatic residues (H188 and F197) are expected to play a central role in the electron-

transfer pathway for the reduction of cyt c_3. In the reduction of the hydrogenase, however, heme 3 in cyt c_3 is suggested to play a key role.

ACKNOWLEDGMENT

We are grateful to Prof. Takahisa Ikegami (Osaka University) for his fruitful discussions on the NMR measurements and to Miss Asuka Nakahara (University of Hyogo) for the help in *Dv*MF cultivation.

SUPPORTING INFORMATION AVAILABLE

^{1}H NMR spectra of all lysine mutant cytochromes c_3 used in this work and chemical shift variations table for ^{1}H and ^{15}N nuclei for ferric and ferrous cytochrome c_3 upon complex formation with [NiFe] hydrogenase. These materials are available free of charge via the Internet at http://pubs.acs.org.

REFERENCES

1. Bento, I., Matias, P. M., Baptista, A. M., da Costa, P. N., van Dongen, W. M., Saraiva, L. M., Schneider, T. R., Soares, C. M., and Carrondo, M. A. (2004) Molecular basis for redox-Bohr and cooperative effects in cytochrome c_3 from *Desulfovibrio desulfuricans* ATCC 27774: crystallographic and modeling studies of oxidized and reduced high-resolution structures at pH 7.6, *Proteins 54*, 135−152.
2. Harada, E., Fukuoka, Y., Ohmura, T., Fukunishi, A., Kawai, G., Fujiwara, T., and Akutsu, H. (2002) Redox-coupled conformational alternations in cytochrome c_3 from *D. vulgaris* Miyazaki F on the basis of its reduced solution structure, *J. Mol. Biol. 319*, 767−778.
3. Correia, I. J., Paquete, C. M., Coelho, A., Almeida, C. C., Catarino, T., Louro, R. O., Frazao, C., Saraiva, L. M., Carrondo, M. A., Turner, D. L., and Xavier, A. V. (2004) Proton-assisted two-electron transfer in natural variants of tetraheme cytochromes from *Desulfomicrobium* Sp., *J. Biol. Chem. 279*, 52227−52237.
4. Park, J.-S., Kano, K., Morimoto, Y., Higuchi, Y., Yasuoka, N., Ogata, M., Niki, K., and Akutsu, H. (1991) ^{1}H NMR studies on ferricytochrome c_3 from *Desulfovibrio vulgaris* Miyazaki F and its interaction with ferredoxin I, *J. Biomol. NMR 1*, 271−282.
5. Dolla, A., Guerlesquin, F., Bruschi, M., and Haser, R. (1991) Ferredoxin electron-transfer site on cytochrome c_3. Structural hypothesis of an intramolecular electron-transfer pathway within a tetra-heme cytochrome, *J. Mol. Recognit. 4*, 27−33.
6. Dolla, A., Leroy, G., Guerlesquin, F., and Bruschi, M. (1991) Identification of the site of interaction between cytochrome c_3 and ferredoxin using peptide mapping of the cross-linked complex, *Biochim. Biophys. Acta 1058*, 171−177.
7. Stewart, D. E., LeGall, J., Moura, I., Moura, J. J. G., Peck, H. D., Jr., Xavier, A. V., Weiner, P. K., and Wampler, J. E. (1988) A hypothetical model of the flavodoxin-tetraheme cytochrome c_3 complex of sulfate-reducing bacteria, *Biochemistry 27*, 2444−2450.
8. Palma, P. N., Moura, I., LeGall, J., Beeumen, J. V., Wampler, J. E., and Moura, J. J. G. (1994) Evidence for a ternary complex formed between flavodoxin and cytochrome c_3: ^{1}H-NMR and molecular modeling studies, *Biochemistry 33*, 6394−6407.
9. Feng, Y., and Swenson, R. P. (1997) Evaluation of the role of specific acidic amino acid residues in electron transfer between the flavodoxin and cytochrome c_3 from *Desulfovibrio vulgaris* [Hildenborough], *Biochemistry 36*, 13617−13628.
10. Correia, C., Monzani, E., Moura, I., Lampreia, J., and Moura, J. J. G. (1999) Cross-linking between cytochrome c_3 and flavodoxin from *Desulfovibrio gigas*, *Biochem. Biophys. Res. Commun. 256*, 367−371.
11. Stewart, D. E., LeGall, J., Moura, I., Moura, J. J. G., Peck, H. D., Jr., Xavier, A. V., Weiner, P. K., and Wampler, J. E. (1989) Electron transfer in sulfate-reducing bacteria: Molecular modeling and NMR studies of the rubredoxin-tetraheme-cytochrome-c_3 complex, *Eur. J. Biochem. 185*, 695−700.
12. Matias, P. M., Saraiva, L. M., Soares, C. M., Coelho, A. V., LeGall, J., and Carrondo, M. A. (1999) Nine-haem cytochrome *c* from *Desulfovibrio desulfuricans* ATCC 27774: primary sequence determination, crystallographic refinement at 1.8 and modeling studies of its interaction with the tetrahaem cytochrome c_3, *J. Biol. Inorg. Chem. 4*, 478−494.
13. Czjzek, M., ElAntak, L., Zamboni, V., Morelli, X., Dolla, A., Guerlesquin, F., and Bruschi, M. (2002) The crystal structure of the hexadeca-heme cytochrome Hmc and a structural model of its complex with cytochrome c_3, *Structure 10*, 1677−1686.
14. Teixeira, V. H., Baptista, A. M., and Soares, C. M. (2004) Modeling electron-transfer thermodynamics in protein complexes: interaction between two cytochromes c_3, *Biophys. J. 86*, 2773−2785.
15. Odom, J. M., and Peck, H. D., Jr. (1981) Hydrogen cycling as a general mechanism for energy coupling in the sulfate-reducing bacteria, *Desulfovibrio* sp., *FEMS Microbiol. Lett. 12*, 47−50.
16. Higuchi, Y., Yagi, T., and Yasuoka, N. (1997) Unusual ligand structure in Ni−Fe active center and an additional Mg site in hydrogenase revealed by high-resolution X-ray structure analysis, *Structure 5*, 1671−1680.
17. Volbeda, A., Charon, M.-H., Piras, C., Hatchikian, E. C., Frey, M., and Fontecilla-Camps, J. C. (1995) Crystal structure of the nickel−iron hydrogenase from *Desulfovibrio gigas*, *Nature 373*, 580−587.
18. Montet, Y., Amara, P., Volbeda, A., Vornede, X., Hatchikian, E. C., Field, M. J., Frey, M., and Fontecilla-Camps, J. C. (1997) Gas access to the active site of Ni−Fe hydrogenase probed by X-ray crystallography and molecular dynamics, *Nat. Struct. Biol. 4*, 523−526.
19. Matias, P. M., Soares, C. M., Saraiva, L. M., Coelho, R., Morais, J., LeGall, J., and Carrondo, M. A. (2001) [NiFe] hydrogenase from *Desulfovibrio desulfuricans* ATCC 27774: gene sequencing, three-dimensional structure determination and refinement at 1.8 Å and modeling studies of its interaction with the tetrahaem cytochrome c_3, *J. Biol. Inorg. Chem.* 6, 63−81.
20. Garcin, E., Vernede, X., Hatchikian, E. C., Volbeda, A., Frey, M., and Fontecilla-Camps, J. C. (1999) The crystal structure of a reduced [NiFeSe] hydrogenase provides an image of the activated catalytic center, *Structure 7*, 557−566.
21. Nicolet, Y., Piras, C., Legrand, P., Hatchikian, C. E., and Fontecilla-Camps, J. C. (1999) *Desulfovibrio desulfuricans* iron hydrogenase: the structure shows unusual coordination to an active site Fe binuclear center, *Structure 7*, 13−23.
22. Peters, J. W., Lanzilotta, W. N., Lemon, B. J., and Seefeldt, L. C., (1998) X-ray crystal structure of the Fe-only hydrogenase (CpI) from *Clostridium pasteurianum* to 1.8 angstrom resolution, *Science 282*, 1853−1858.
23. Brugna, M., Giudici-Orticoni, M. T., Spinelli, S., Brown, K., Tegoni, M., and Bruschi, M. (1998) Kinetics and interaction studies between cytochrome c_3 and Fe-only hydrogenase from *Desulfovibrio vulgaris* Hildenborough, *Proteins 33*, 590−600.
24. Dolla, A., Arnoux, P., Protasevich, I., Lobachov, V., Brugna, M., Giudici-Orticoni, M. T., Haser, R., Czjzek, M., Makarov, A., and Bruschi, M. (1999) Key role of phenylalanine 20 in cytochrome c_3: structure, stability, and function studies, *Biochemistry 38*, 33−41.
25. ElAntak, L., Morelli, X., Bornet, O., Hatchikian, C., Czjzek, M., Dolla, A., and Guerlesquin, F. (2003) The cytochrome c_3−[Fe]-hydrogenase electron-transfer complex: structural model by NMR restrained docking, *FEBS Lett. 548*, 1−4.
26. Aubert, C., Leroy, G., Bruschi, M., Wall, J. D., and Dolla, A. (1997) A single mutation in the heme 4 environment of *Desulfovibrio desulfuricans* Norway cytochrome c_3 (M_r 26,000) greatly affects the molecular reactivity, *J. Biol. Chem. 272*, 15128−15134.
27. Aubert, C., Giudici-Orticoni, M.-T., Czjzek, M., Haser, R., Bruschi, M., and Dolla, A. (1998) Structural and kinetic studies of the Y73E mutant of octaheme cytochrome c_3 (M_r = 26 000) from *Desulfovibrio desulfuricans Norway*, *Biochemistry 37*, 2120−2130.
28. Chen, R., and Weng, Z. (2003) A novel shape complementarity scoring function for protein−protein docking, *Proteins 51*, 397−408.
29. Ozawa, K., Takayama, Y., Yasukawa, F., Ohmura, T., Cusanovich, M. A., Tomimoto, Y., Ogata, H., Higuchi, Y., and Akutsu, H. (2003) Role of the aromatic ring of Tyr43 in tetraheme cytochrome c_3 from *Desulfovibrio vulgaris* Miyazaki F, *Biophys. J. 85*, 3367−3374.
30. Ozawa, K., Yasukawa, F., Fujiwara, Y., and Akutsu, H. (2001) A simple, rapid, and highly efficient gene expression system for multiheme cytochromes *c*, *Biosci., Biotechnol., Biochem. 65*, 185−189.

31. Takayama, Y., Harada, E., Kobayashi, R., Ozawa, K., and Akutsu, H. (2004) Roles of noncoordinated aromatic residues in redox regulation of cytochrome c_3 from *Desulfovibrio vulgrais* Miyazaki F, *Biochemistry 43*, 10859−10866.
32. Postgate, J. R. (1984) *The Sulfate-Reducing Bacteria*, 2nd ed., pp 32, Cambridge University Press, Cambridge, U.K.
33. Ozawa, K., Mogi, T., Suzuki, M., Kitamura, M., Nakaya, T., Anraku, Y., and Akutsu, H. (1997) Membrane-bound cytochromes in a sulfate-reducing strict anaerobe *Desulfovibrio vulgaris* Miyazaki F, *Anaerobe 3*, 339−346.
34. Hubbard, S. J., and Thornton, J. M. (1993) 'NACCESS', computer program, Department of Biochemistry and Molecular Biology, University College London.
35. Brunger, A. T. (1992) X-PLOR, Version 3.1, A system for X-ray crystallography and NMR, Yale University Press, New Haven, CT.
36. Powell, M. J. D. (1977) Restart procedures for the conjugate gradient method, *Math. Program. 12*, 241−254.
37. Niki, K., Kobayashi, Y., and Matsuda, H. (1984) Determination of macroscopic standard potentials of a molecule with a reversible *n*-consecutive one-electron-transfer process. Application to a tetraheme protein: cytochrome c_3, *J. Electroanal. Chem. 178*, 333−341.
38. Rousset, M., Montet, Y., Guigliarelli, B., Forget, N., Asso, M., Bertrand, P., Fontecilla-Camps, J. C., and Hatchikian, C. (1998) [3Fe-4S] to [4Fe-4S] cluster conversion in *Desulfovibrio fructosovorans* [NiFe] hydrogenase by site-directed mutagenesis, *Proc. Natl. Acad. Sci. U.S.A. 95*, 11625−11630.
39. Park, J.-S., Ohmura, T., Kano, K., Sagara, T., Niki, K., Kyogoku, Y., and Akutsu, H. (1996) Regulation of the redox order of four hemes by pH in cytochrome c_3 from *D. vulgaris* Miyazaki F, *Biochim. Biophys. Acta 1293*, 45−54.
40. Higuchi, Y., Ogata, H., Miki, K., Yasuoka, N., and Yagi, T. (1999) Removal of the binding ligand atom at the Ni−Fe active site of [NiFe] hydrogenase upon reduction with H_2, as revealed by X-ray structure analysis at 1.4 Å resolution, *Structure 7*, 549−556.
41. Morelli, X., Czjzek, M., Hatchikian, C. E., Bornet, O., Fontecilla-Camps, J. C., Palma, N. P., Moura, J. J. G., and Guerlesquin, F. (2000) Structural model of the Fe-hydrogenase/cytochrome c_{553} complex combining transverse relaxation-optimized spectroscopy experiments and soft docking calculations, *J. Biol. Chem. 275*, 23204−23210.
42. Page, C. C., Moser, C. C., Chen, X., and Dutton, L. (1999) Natural engineering principles of electron tunnelling in biological oxidation−reduction, *Nature 402*, 47−52.
43. Vignais, P. M., Billoud, B., and Meyer, J. (2001) Classification and phylogeny of hydrogenases, *FEMS Microbiol. Rev. 25*, 455−501.
44. Nicholls, A., Sharp, K. A., and Honig, B. (1991) Protein folding and association: insights from the interfacial and thermodynamic properties of hydrocarbons, *Proteins 11*, 281−296.

BI0514360